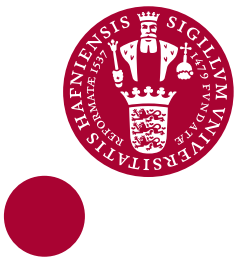

Hidden or missing outflows in highly obscured galaxy nuclei?

Falstad, N.; Hallqvist, F.; Aalto, S.; Konig, S.; Muller, S.; Aladro, R.; Combes, F.; Evans, A. S.; Fuller, G. A.; Gallagher, J. S.; Garcia-Burillo, S.; Gonzalez-Alfonso, E.; Greve, T. R.; Henkel, C.; Imanishi, M.; Izumi, T.; Mangum, J. G.; Martin, S.; Privon, G. C.; Sakamoto, K.; Veilleux, S.; van der Werf, P. P.

Published in:
Astronomy & Astrophysics

DOI:
10.1051/0004-6361/201834586

Publication date:
2019

Document version
Publisher's PDF, also known as Version of record

A&A 623, A29 (2019)
https://doi.org/10.1051/0004-6361/201834586

Astronomy & Astrophysics

Hidden or missing outflows in highly obscured galaxy nuclei?⋆

N. Falstad[1], F. Hallqvist[1], S. Aalto[1], S. König[1], S. Muller[1], R. Aladro[2], F. Combes[3], A. S. Evans[4,5], G. A. Fuller[6], J. S. Gallagher[7], S. García-Burillo[8], E. González-Alfonso[9], T. R. Greve[10,11], C. Henkel[2,12], M. Imanishi[13], T. Izumi[13], J. G. Mangum[4], S. Martín[14,15], G. C. Privon[16], K. Sakamoto[17], S. Veilleux[18], and P. P. van der Werf[19]

[1] Department of Space, Earth and Environment, Chalmers University of Technology, Onsala Space Observatory, 439 92 Onsala, Sweden
e-mail: niklas.falstad@chalmers.se
[2] Max-Planck-Institut für Radioastronomie, Auf dem Hügel 69, 53121 Bonn, Germany
[3] Observatoire de Paris, LERMA, College de France, CNRS, PSL Univ., UPMC, Sorbonne Univ., 75014 Paris, France
[4] National Radio Astronomy Observatory, 520 Edgemont Road, Charlottesville, VA 22903, USA
[5] Department of Astronomy, 530 McCormick Road, University of Virginia, Charlottesville, VA 22904, USA
[6] Jodrell Bank Centre for Astrophysics, School of Physics & Astronomy, The University of Manchester, Oxford Road, Manchester M13 9PL, UK
[7] Department of Astronomy, University of Wisconsin-Madison, 5534 Sterling, 475 North Charter Street, Madison, WI 53706, USA
[8] Observatorio de Madrid, OAN-IGN, Alfonso XII, 3, 28014 Madrid, Spain
[9] Universidad de Alcalá, Departamento de Física y Matemáticas, Campus Universitario, 28871 Alcalá de Henares, Madrid, Spain
[10] Cosmic Dawn Center (DAWN), DTU-Space, Technical University of Denmark, Elektrovej 327, 2800 Kgs. Lyngby; Niels Bohr Institute, University of Copenhagen, Juliane Maries Vej 30, 2100 Copenhagen, Denmark
[11] Department of Physics and Astronomy, University College London, Gower Street, London WC1E 6BT, UK
[12] Astron. Dept., King Abdulaziz University, PO Box 80203, 21589 Jeddah, Saudi Arabia
[13] National Astronomical Observatory of Japan, National Institutes of Natural Sciences (NINS), 2-21-1 Osawa, Mitaka, Tokyo 181–8588, Japan
[14] European Southern Observatory, Alonso de Córdova 3107, Vitacura 763 0355, Santiago, Chile
[15] Joint ALMA Observatory, Alonso de Córdova 3107, Vitacura 763 0355, Santiago, Chile
[16] Department of Astronomy, University of Florida, 211 Bryant Space Sciences Center, Gainesville, FL 32611, USA
[17] Institute of Astronomy and Astrophysics, Academia Sinica, PO Box 23-141, 10617, Taipei, Taiwan
[18] Department of Astronomy, University of Maryland, College Park, MD 20742, USA
[19] Leiden Observatory, Leiden University, PO Box 9513, 2300 RA Leiden, The Netherlands

Received 6 November 2018 / Accepted 17 January 2019

ABSTRACT

Context. Understanding the nuclear growth and feedback processes in galaxies requires investigating their often obscured central regions. One way to do this is to use (sub)millimeter line emission from vibrationally excited HCN (HCN-vib), which is thought to trace warm and highly enshrouded galaxy nuclei. It has been suggested that the most intense HCN-vib emission from a galaxy is connected to a phase of nuclear growth that occurs before the nuclear feedback processes have been fully developed.
Aims. We aim to investigate if there is a connection between the presence of strong HCN-vib emission and the development of feedback in (ultra)luminous infrared galaxies ((U)LIRGs).
Methods. We collected literature and archival data to compare the luminosities of rotational lines of HCN-vib, normalized to the total infrared luminosity, to the median velocities of 119 μm OH absorption lines, potentially indicating outflows, in a total of 17 (U)LIRGs.
Results. The most HCN-vib luminous systems all lack signatures of significant molecular outflows in the far-infrared OH absorption lines. However, at least some of the systems with bright HCN-vib emission have fast and collimated outflows that can be seen in spectral lines at longer wavelengths, including in millimeter emission lines of CO and HCN (in its vibrational ground state) and in radio absorption lines of OH.
Conclusions. We conclude that the galaxy nuclei with the highest $L_{\rm HCN-vib}/L_{\rm IR}$ do not drive wide-angle outflows that are detectable using the median velocities of far-infrared OH absorption lines. This is possibly because of an orientation effect in which sources oriented in such a way that their outflows are not along our line of sight also radiate a smaller proportion of their infrared luminosity in our direction. It could also be that massive wide-angle outflows destroy the deeply embedded regions responsible for bright HCN-vib emission, so that the two phenomena cannot coexist. This would strengthen the idea that vibrationally excited HCN traces a heavily obscured stage of evolution before nuclear feedback mechanisms are fully developed.

Key words. galaxies: evolution – galaxies: nuclei – galaxies: ISM – ISM: molecules – ISM: jets and outflows

⋆ *Herschel* is an ESA space observatory with science instruments provided by European-led Principal Investigator consortia and with important participation from NASA.

1. Introduction

Luminous and ultraluminous infrared galaxies ((U)LIRGs) are gas-rich systems that radiate intensely in the infrared portion of the electromagnetic spectrum and have infrared luminosities ($L_{\rm IR} = L(8-1000\,\mu{\rm m})$) in excess of $10^{11}\,L_\odot$ and $10^{12}\,L_\odot$, respectively (e.g., Sanders & Mirabel 1996). These large luminosities are due to dust-reprocessed radiation from intense star formation, an active galactic nucleus (AGN), or both. In the local Universe, (U)LIRGs are relatively rare compared to less luminous objects, but surveys at millimeter and submillimeter wavelengths have shown that they are much more numerous at high redshifts (e.g., Smail et al. 1997; Hughes et al. 1998), indicating that they play an important role in the evolution of galaxies. Two important questions in this context are as follows: How did the supermassive black holes (SMBHs) found in the nuclei of most galaxies grow, and how are they related to the evolution of their host galaxies? From observations, we know that tight relations between the mass of the central SMBH and various properties of the host galaxy exist in large ellipticals (e.g., Magorrian et al. 1998; Ferrarese & Merritt 2000; Gebhardt et al. 2000; Kormendy & Ho 2013). It has been suggested that these relations were partly established through a process, mostly taking place in the early Universe, in which galaxies of similar masses collide and merge (see, e.g., Kormendy & Ho 2013, for a review). In such mergers, large amounts of gas are funneled into the new nucleus, giving rise to intense starbursts, AGN activity, or both. The exact physics of how the black hole-host relations would be established is still obscure, but several suggested galaxy merger scenarios include a starburst-dominated phase followed by a phase of obscured AGN activity. Eventually, the AGN becomes strong enough to drive outflows that clear the surrounding material and reveal the central activity (e.g., Sanders et al. 1988a; Hopkins et al. 2006; Urrutia et al. 2008; Simpson et al. 2012). Thus, studies of the most dust-embedded phase of evolution and the early stages of feedback are essential to understand how SMBHs grow together with their host galaxies.

However, observations of the most enshrouded galaxy nuclei are hampered by the large amounts of obscuring material that surround them. One solution to this problem is to observe at millimeter and radio wavelengths, where the dust is less optically thick (e.g., Barcos-Muñoz et al. 2015). Some common tracers of obscured galaxy nuclei at these wavelengths are the low-J rotational lines of the HCN and HCO^+ molecules. Recently, however, it has been shown that, in the most obscured systems, even these dense-gas tracers are heavily affected by continuum- and/or self-absorption by cooler foreground gas (e.g., Sakamoto et al. 2009; Aalto et al. 2015a; Martín et al. 2016). A better suited tracer of the most obscured systems is offered by HCN in its first vibrationally excited state, $v_2 = 1$ (hereafter HCN-vib). Strong emission lines from rotational transitions within the $v_2 = 1$ state have been detected in external galaxies at (sub)millimeter wavelengths, first by Sakamoto et al. (2010) and then in many subsequent observations. With energy levels that lie more than 1000 K above the ground state, HCN-vib is mainly excited by absorption of mid-infrared radiation. However, to be efficiently populated this emission line requires brightness temperatures in excess of 100 K at 14 μm, which is the wavelength of the transition between the ground and first vibrationally excited states of HCN; this translates into a H_2 column density larger than $2 \times 10^{23}\,{\rm cm}^{-2}$ for a dust temperature of 100 K (Aalto et al. 2015a). This makes bright HCN-vib emission an excellent unabsorbed (Martín et al. 2016) tracer of high column density gas with high mid-infrared surface brightness. While the direct mid-infrared radiation from such regions is often hidden from us by the large quantities of obscuring material, the rotational transitions inside the vibrationally excited states occur at millimeter and submillimeter wavelengths where the dust opacity is lower. The low-J rotational lines of HCN-vib are thus useful probes of the nuclear mid-infrared source in heavily obscured objects. Since the first extragalactic (sub)millimeter detection of HCN-vib rotational line emission by Sakamoto et al. (2010), the field has developed rapidly (e.g., Imanishi & Nakanishi 2013; Aalto et al. 2015a,b; Imanishi et al. 2016a,b, 2018; Martín et al. 2016), notably thanks to the Atacama Large Millimeter/submillimeter Array (ALMA).

In their study of HCN-vib in obscured galaxies, Aalto et al. (2015a) found that all galaxies with detected HCN-vib emission show evidence of inflows, outflows, or both. In addition, they found a tentative trend that galaxies with fast molecular outflows have fainter HCN-vib emission relative to their total infrared luminosity. The trend is especially striking when comparing the strength of the HCN-vib emission to the velocity of the wide-angle OH outflows studied by, for example, Veilleux et al. (2013). Based on a relatively small sample of nine galaxies, Aalto et al. (2015a) tentatively suggested that strong HCN-vib emission is connected to a rapid phase of nuclear growth that occurs right before the onset of strong feedback.

In this paper, we present the results of a study employing a sample of 19 galaxies including data from the literature as well as previously unpublished data to further investigate the connection, or lack thereof, between strong HCN-vib emission and molecular outflows. The sample used in this study is described in Sect. 2 and in Sect. 3 we present the results, which are then discussed in Sect. 4. Finally, the conclusions that we draw from the analysis are summarized in Sect. 5. Throughout the paper, a $H_0 = 73\,{\rm km\,s^{-1}\,Mpc^{-1}}$, $\Omega_{\rm m} = 0.27$, and $\Omega_\Lambda = 0.73$ cosmology is adopted.

2. Sample

We searched for (U)LIRGs with existing ALMA observations of HCN-vib that are either already published or that have the data publicly available in the the ALMA science archive[1]. In addition, we included published HCN-vib observations taken with the Plateau de Bure Interferometer (PdBI), the Northern Extended Millimeter Array (NOEMA), or the Submillimeter Array (SMA). We did not include nondetections unless they have existing observations of the OH doublet at 119 μm, which we use to determine the outflow velocity. We also excluded nondetections when a meaningful upper limit to the HCN-vib flux could not be determined, owing either to low sensitivity spectra or significant flux from the HCO^+ line, which is separated from HCN-vib by $\sim$400 km s^{-1}. This is a possible source of bias, as HCN-vib emission may be hidden by the HCO^+ line in sources with outflowing gas. In practice, most sources that have been excluded either do not have any outflow signatures in the far-infrared OH lines that we use to trace outflows (see below) or they have not been observed in these lines. The two exceptions are IRAS 19254–7245 (Imanishi et al. 2016a) and NGC 6240 (ALMA project 2015.1.01448.S, PI: R. Tunnard), in which the median velocities of the OH 119 μm lines are ~-250 and ~-200 km s^{-1}, respectively. In total, we excluded ten sources, most of which are due to lack of OH measurements.

For consistency of the sample, we ensured that outflow velocities were measured using the same common tracers and

[1] The ALMA science archive is available at https://almascience.nrao.edu/alma-data/archive

Table 1. Sample galaxies.

Name	Type[a]	z[b]	D_L[c] (Mpc)	L_{IR}[d] ($10^{11}\,L_\odot$)
NGC 4418	Sy 2	0.0071	33.6 ± 2.5	1.32 ± 0.19
IC 860	H II	0.0130	62.1 ± 4.3	1.60 ± 0.22
IRAS 12224–0624	L	0.0264	119.5 ± 8.2	1.98 ± 0.27
Zw 049.057	H II	0.0130	62.4 ± 4.3	2.04 ± 0.28
NGC 7469	Sy 1	0.0164	68.2 ± 4.7	4.13 ± 0.57
I Zw 1	Sy 1	0.0610	258.2 ± 17.7	8.22 ± 1.13
UGC 5101	L	0.0394	169.7 ± 11.6	9.50 ± 1.30
IRAS 20551–4250	H II	0.0430	185.2 ± 12.7	10.65 ± 1.46
IRAS 15250+3609	L	0.0552	243.7 ± 16.7	11.08 ± 1.53
IRAS 08572+3915	L	0.0584	253.1 ± 17.3	13.38 ± 1.84
IRAS 05189–2524	Sy 2	0.0428	180.2 ± 12.4	13.50 ± 1.85
IRAS 22491–1808	H II	0.0778	337.0 ± 23.1	13.88 ± 1.92
Mrk 273	Sy 2	0.0378	165.6 ± 11.3	14.81 ± 2.03
IRAS 20414–1651	H II	0.0871	383.4 ± 26.3	15.12 ± 2.18
Arp 220	L	0.0181	84.1 ± 5.8	17.25 ± 2.36
IRAS 13120–5453	Sy 2	0.0308	137.8 ± 9.5	19.20 ± 2.65
IRAS 12112+0305	L	0.0733	326.3 ± 22.4	20.35 ± 2.79
IRAS 17208–0014	H II	0.0428	189.3 ± 13.0	26.21 ± 3.59
Mrk 231	Sy 1	0.0422	184.3 ± 12.6	34.30 ± 4.70

Notes. [(a)]Optical spectral types H II, L (for LINER), Sy 1 and Sy 2 (for Seyfert 1 and 2, respectively). When available, we used the classifications from Veilleux et al. (1995) and Kim et al. (1998), otherwise, we used classifications from Sanders et al. (1988b), Baan et al. (1998), and Véron-Cetty & Véron (2001). [(b)]In priority order, we used redshifts from Veilleux et al. (2013), Sanders et al. (2003), or Strauss et al. (1992), except for IRAS 05189–2524 where the redshift from Sanders et al. (1991) was used. [(c)]Luminosity distances were calculated from the redshifts following the same procedure as Sanders et al. (2003). [(d)]Infrared luminosities were calculated using the prescription in Table 1 of Sanders & Mirabel (1996; originally from Pérault 1987) using IRAS fluxes taken from Sanders et al. (2003), except for IRAS 20414–1651 where fluxes were taken from Moshir et al. (1992), and I Zw 1 where they were taken from Sanders et al. (1989).

following the same procedures. We therefore checked all sources with HCN-vib observations for observations of the far-infrared OH doublet at 119 μm with the *Herschel* Space Observatory (Pilbratt et al. 2010) as this is a known tracer of molecular outflows on subkiloparsec scales, which has been observed in a large number of (U)LIRGs (e.g., Fischer et al. 2010; Veilleux et al. 2013; González-Alfonso et al. 2017a). The OH molecule has high abundances in photodissociation regions as well as in X-ray dominated regions (e.g., Maloney et al. 1996; Goicoechea et al. 2011; Meijerink et al. 2011). Unlike other common outflow tracers like the millimeter rotational transitions of CO and HCN, the ground state OH 119 μm doublet is often detected in absorption toward the far-infrared background (e.g., Veilleux et al. 2013), providing an unambiguous tracer of the gas motion. The transitions between excited states (for example, the doublets at 65 and 84 μm) are generally weaker and the line wings are not always detected (González-Alfonso et al. 2017a). Recently, the 119 μm doublet was also used to detect a fast outflow ($\lesssim$800 km s^{-1}) in a galaxy at a redshift of 5.3 (Spilker et al. 2018). Systematic searches of outflow signatures in the far-infrared OH lines have revealed evidence of molecular outflows in approximately two-thirds of the observed (U)LIRG samples (Veilleux et al. 2013; Spoon et al. 2013). From this detection rate, Veilleux et al. (2013) inferred a wide average opening angle of ∼145°, assuming that all objects in their sample have outflows. In fact, based on radiative transfer models and spatially resolved observations of two outflows, González-Alfonso et al. (2017a) argued that the 119 μm OH absorptions are primarily sensitive to wide-angle outflows. On the other hand, unambiguous signatures of inflows are only found in one-tenth of the sources in the sample of Veilleux et al. (2013), suggesting that OH inflows are either rare or have, on average, smaller opening angles.

In particular, the 43 sources in the far-infrared OH sample of Veilleux et al. (2013) were checked for observations of the (sub)millimeter HCN-vib J = 3−2 or J = 4−3 lines. Fourteen of these had HCN-vib detections or data that allowed for meaningful upper limits to be estimated. One of them, IRAS 05189–2524 (see Appendix B), has previously unpublished data in the ALMA science archive while data for the remaining 13 were taken from Sakamoto et al. (2010), Aalto et al. (2015b,a), Imanishi et al. (2016a,b), Martín et al. (2016), Privon et al. (2017), Aladro et al. (2018), and König et al. (in prep.). In addition, five sources not included in the sample of Veilleux et al. (2013) were found to have usable observations of HCN-vib. One, IRAS 12224–0624 (see Appendix B), has previously unpublished data in the ALMA science archive while the other four were taken from Aalto et al. (2015a) and Imanishi et al. (2016a). Three of these five sources, Zw 049.057, IRAS 20414–1651, and NGC 7469, also have existing observations of the OH 119 μm doublet (see Appendix C).

In total, 19 (U)LIRGs with existing HCN-vib observations were found. Of these, 17 also have observations of the OH 119 μm doublet. The final sample, with the adopted redshift and distance of each source, is presented in Table 1.

3. Results

Vibrationally excited HCN luminosities, $L_{\rm HCN-vib}/L_{\rm IR}$ ratios, and OH median velocities are presented in Table 2. We adopt the $L_{\rm HCN-vib}/L_{\rm IR}$ ratio as a parameter to describe the strength of HCN-vib in a normalized fashion. However, we are aware that some part of the total $L_{\rm IR}$ may be unrelated to the dusty nucleus, and instead may come from, for example, an extended starburst. In particular, in systems with multiple nuclei, for example Arp 220 and IRAS 12112+0305, $L_{\rm IR}$ has contributions from both nuclei. In our sample, we are not aware of any sources for which these effects would affect the $L_{\rm HCN-vib}/L_{\rm IR}$ ratio enough to change our results significantly. We use the median velocity of the OH lines instead of the terminal outflow velocity as the former provides more robust values (Veilleux et al. 2013). Velocities are only given for those sources with absorption in the OH 119 μm doublet, as this means that the gas is in the foreground and that a positive or negative velocity shift can be interpreted as evidence of gas moving toward or away from the background nucleus, respectively. We note that this does not necessarily indicate in- or outflowing gas in all cases as, for example, interactions between two nuclei can also affect the OH kinematics. In addition, it is important to take the uncertainties in the velocity determination into account. For example, Veilleux et al. (2013) defined an outflow as having an OH absorption feature with a median velocity more negative than −50 km s^{-1}, which is the typical uncertainty on the velocities. The requirement to detect the OH doublet in absorption is a possible source of bias as this requires a high enough column density of OH in front of a strong enough far-infrared background source. However, we note that all galaxies with an HCN-vib detection, if observed, were also detected in absorption in the OH 119 μm doublet. Therefore, we did not miss any sources with a combination of high HCN-vib luminosity and a fast outflow because of this effect.

Table 2. $L_{\rm HCN-vib}$ and outflow properties.

Name	$L_{\rm HCN-vib}$ ($10^3\,L_\odot$)	$L_{\rm HCN-vib}/L_{\rm IR}$ (10^{-8})	v_{50}(abs)[a] (km s^{-1})	Observatory	References
$J = 3-2$					
NGC 4418	5.0 ± 1.2	3.77 ± 0.71	111	SMA	1
IC 860	4.2 ± 0.8	2.65 ± 0.37	not obs.	PdBI	2
Zw 049.057	7.3 ± 2.0	3.57 ± 0.76	37	PdBI	2
NGC 7469	<0.1	<0.03	emi.	ALMA	3
I Zw 1	<1.7	<0.21	emi.	ALMA	3
UGC 5101	20.5 ± 5.5	2.15 ± 0.50	−9	NOEMA	4
IRAS 20551–4250	2.3 ± 0.7	0.21 ± 0.06	−381	ALMA	5
IRAS 15250+3609	<11.3[b]	<1.02	189	ALMA	3
IRAS 08572+3915 NW	<6.4	<0.48	−489	ALMA	3
IRAS 22491–1808 E	13.2 ± 3.9	0.95 ± 0.25	99	ALMA	3
Mrk 273	<16.9	<1.14	−201	NOEMA	6
IRAS 20414-1651	<7.5	<0.50	−32	ALMA	3
Arp 220 W	40.9 ± 7.0	2.37 ± 0.25[c]	21	ALMA	7
Arp 220 E	8.9 ± 1.5	0.51 ± 0.05[c]	21	ALMA	7
IRAS 12112+0305 NE	14.3 ± 4.0	0.70 ± 0.17[c]	−117	ALMA	3
Mrk 231	14.5 ± 3.1	0.42 ± 0.07	−237	PdBI	8
$J = 4-3$					
NGC 4418	12.4 ± 2.5	9.41 ± 1.25	111	SMA	1
IRAS 12224–0624	16.9 ± 4.5	8.52 ± 1.95	not obs.	ALMA	9
IRAS 20551–4250	4.8 ± 1.2	0.45 ± 0.09	−381	ALMA	10
IRAS 05189–2524	8.0 ± 2.7	0.59 ± 0.18	−387[d]	ALMA	9
Arp 220 W	108.1 ± 19.9	6.27 ± 0.77	21	ALMA	7
Arp 220 E	25.8 ± 4.4	1.49 ± 0.15	21	ALMA	7
IRAS 13120–5453	<5.5	<0.29	−195	ALMA	11
IRAS 17208–0014	101.9 ± 17.5	3.89 ± 0.40	51	ALMA	2

Notes. [(a)]Median OH outflow velocities taken from Veilleux et al. (2013) or, for sources not in their sample, from archival data following the same procedure. Sources that were not observed or where the doublet was detected in emission are indicated with not obs. or emi., respectively. The typical uncertainty on the velocities is 50 km s^{-1}. [(b)]Imanishi et al. (2016a) interpreted an emission feature at the position of the HCN-vib line as a subpeak of the nearby HCO$^+$ line. We use this value as an upper limit to the HCN-vib luminosity. [(c)]The $L_{\rm HCN-vib}/L_{\rm IR}$ is calculated using the total $L_{\rm IR}$ of the system, possibly introducing some bias in systems with multiple nuclei. [(d)]The median velocity of the lines in IRAS 05189–2524 is adjusted to correct for the different redshift adopted compared to that used by Veilleux et al. (2013).
References. (1) Sakamoto et al. (2010); (2) Aalto et al. (2015a); (3) Imanishi et al. (2016a); (4) König et al. (in prep.); (5) Imanishi et al. (2016b); (6) Aladro et al. (2018); (7) Martín et al. (2016); (8) Aalto et al. (2015b); (9) This work; (10) Imanishi & Nakanishi (2013); (11) Privon et al. (2017).

The line luminosities presented in Table 2 are calculated following Eq. (1) in Solomon & Vanden Bout (2005), applied to HCN-vib:

$$L_{\rm HCN-vib} = 1.04 \times 10^{-3} S_{\rm HCN-vib}\,\Delta v\,\nu_{\rm rest}(1+z)^{-1} D_{\rm L}^2, \quad (1)$$

where $L_{\rm HCN-vib}$ is the HCN-vib luminosity measured in $L_\odot$, $S_{\rm HCN-vib}\,\Delta v$ is the velocity integrated flux in Jy km s^{-1}, $\nu_{\rm rest}$ is the rest frequency in GHz, and $D_{\rm L}$ is the luminosity distance in Mpc. Because of differences in the adopted redshifts and distances, these values differ slightly from those given in the original reference for some of the sources. In case of nondetections, we include the 3σ upper limit to the line luminosity. In the case of IRAS 15250+3609, the HCN-vib line is likely blended with a potential outflow signature in the nearby HCO$^+$ line. We attribute the entire emission feature to the HCN-vib line, and the value given should be considered an upper limit to the HCN-vib luminosity. A short discussion of this source as well as descriptions of the analysis of previously unpublished HCN-vib observations and new OH outflow measurements can be found in Appendices A–C.

In Fig. 1, the OH absorption median velocities are plotted against the luminosities of the HCN-vib line, normalized to the total infrared luminosity of each galaxy. When available, the $J = 3-2$ line is chosen. In the four sources where both transitions are observed, the luminosity ratio of the $J = 4-3$ to $J = 3-2$ lines lies in the range 2–3, with a mean of 2.5. For sources where only the $J = 4-3$ line is observed, we therefore divide its luminosity by 2.5 and include it in the plot with an extra 20% uncertainty added in quadrature. The two galaxies with only emission in the 119 μm doublet, I Zw 1 and NGC 7469, are not included in the plot, but we note that neither of these have an HCN-vib detection.

In the plot in Fig. 1 we see that in our sample the sources with high $L_{\rm HCN-vib}/L_{\rm IR}$ ratios, in excess of 10^{-8}, all lack fast outflows as traced by the median velocity of the OH 119 μm doublet. However, galaxies without fast outflows do not necessarily have high $L_{\rm HCN-vib}/L_{\rm IR}$ ratios. The lack of sources in the upper left portion of the diagram is likely due to selection effects; that area should be populated by less obscured sources of lower luminosity that are not able to drive outflows or provide the necessary conditions for efficient HCN-vib excitation.

4. Discussion

Our comparison of HCN-vib line luminosities and OH 119 μm absorption line velocities in nearby (U)LIRGs shows a trend of

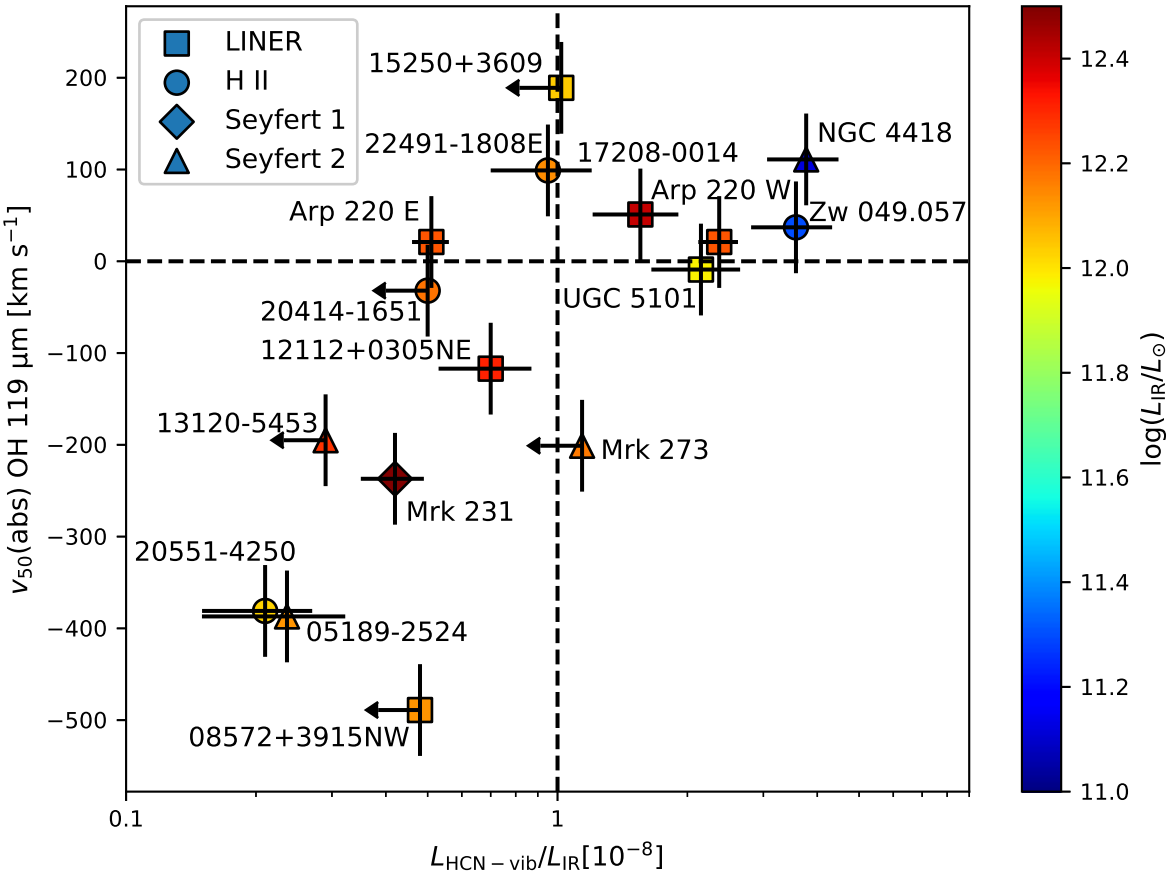

Fig. 1. Median OH absorption velocity as a function of the HCN-vib luminosity relative to the total infrared luminosity. For sources with observations of the $J = 3{-}2$ transition, only this line is plotted. For sources with detections only in the $J = 4{-}3$ line, the HCN-vib luminosity is scaled down by a factor of 2.5, with an extra uncertainty of 20% included in the error bars. Squares, circles, diamonds, and triangles represent LINER, H II, Seyfert 1, and Seyfert 2 optical spectral types, respectively. Colors indicate the total infrared luminosity of each system. Upper limits (3σ) are indicated with arrows.

positive or low negative velocities, indicating inflows or slow outflows in sources with bright HCN-vib emission relative to the total infrared luminosity. This might indicate that regions with the high mid-infrared brightness temperatures required for efficient population of HCN-vib are not affected by inflowing gas, but are destroyed by or cannot form in the presence of strong outflows. In this section, we discuss possible reasons for the lack of outflow signatures in the OH 119 μm absorptions in HCN-vib luminous sources and how the HCN-vib lines relate to other tracers of heavily obscured regions.

4.1. Why do HCN-vib luminous galaxies lack outflow signatures in far-infrared OH lines?

There are several scenarios that could explain the lack of outflow signatures in the galaxies that have bright HCN-vib emission. One such scenario is that there are no outflows, another that the outflows are hidden from detection using the median velocity of the OH 119 μm absorption lines, and a third is that the distribution in Fig. 1 is from orientation effects. These scenarios are discussed in the following sections. We also briefly discuss a possible evolutionary scenario in which the HCN-vib luminous galaxies are in a pre-feedback phase. Admittedly, our sample is very heterogeneous in that it contains galaxies of different merger types, in different merger stages, of different optical classifications, and with infrared luminosities spanning more than an order of magnitude. It is therefore possible that there are several independent reasons for the lack of far-infrared outflow signatures in HCN-vib luminous galaxies.

4.1.1. No outflows

If there are no outflows, it might be because HCN-vib luminous galaxies are intrinsically different from galaxies with weaker HCN-vib emission. For example, Veilleux et al. (2013) found a tendency for systems with dominant AGN to have faster OH outflows; it might then be that the HCN-vib luminous systems, which do not show fast OH outflows, are instead starburst dominated. Indeed, in the two sources with the highest absolute HCN-vib luminosities, IRAS 17208–0014 and Arp 220, less than 10% of the bolometric luminosities are estimated to come from AGN activity based on the 15 to 30 μm continuum ratio (Veilleux et al. 2013). However, this diagnostic can be misleading in galaxies in which the nuclei are optically thick into the far-infrared. Furthermore, at least two other sources with strong HCN-vib emission, NGC 4418 and UGC 5101, have AGN fractions $\gtrsim$50%. While the uncertainty on the AGN fraction determined in this way is estimated to be 20% on average, it is likely much higher in the strongly buried sources discussed in this work.

Another possible explanation for a real lack of outflows in some sources is that we are witnessing a pre-feedback phase in young systems that will later evolve into objects with weak HCN-vib emission and fast outflows. This possibility is discussed

further in Sect. 4.1.4. As discussed by González-Alfonso et al. (2017a), the lack of outflows could also be because, in the most extremely buried sources, it is difficult to find paths with more moderate columns that can be efficiently accelerated to high velocities.

Interestingly, as Aalto et al. (2015a) noted, fast molecular outflows have been found with other tracers and at longer wavelengths in some of the HCN-vib luminous systems. For example, a compact $v > 800\,\mathrm{km\,s^{-1}}$ CO $J = 2{-}1$ outflow has been found in the ULIRG IRAS 17208–0014 (García-Burillo et al. 2015) and an equally fast, compact, and collimated, HCN $J = 1{-}0$ outflow has been detected in the ULIRG Arp 220 (Barcos-Muñoz et al. 2018). Possible outflow signatures have also been found in Zw 049.057 (Falstad et al. 2018) and in NGC 4418 and IRAS 22491–1808 (Fluetsch et al. 2018), although at lower velocities. If we also consider the fact that UGC 5101 has faint high-velocity wings in its OH 119 μm absorption lines (Veilleux et al. 2013), it turns out that all of the six most HCN-vib luminous sources have signatures of molecular outflows.

4.1.2. Obscured, episodic, or collimated outflows

For the HCN-vib bright systems that have outflows, there must be a reason why we do not see them in the far-infrared OH absorption lines. One possibility is that these objects have extreme optical depths in the far-infrared dust continuum, so that much of the outflowing gas cannot be seen owing to obscuration by the dust. In at least some of the sources, high optical depths have indeed been inferred from radiative transfer modeling of *Herschel* observations (e.g., González-Alfonso et al. 2012; Falstad et al. 2015). If this is combined with young outflows that are still very compact, any signatures of these outflows may be completely hidden in the far-infrared. In such a situation, inflows on larger scales, such as that seen in Arp 299A (Falstad et al. 2017), may still be detectable. In fact, at least three of the five most obscured sources (Arp 220, IRAS 17208–0014, and Zw 049.057; Baan et al. 1989; Falstad et al. 2018) have outflows that are seen in the OH lines at centimeter wavelengths but not in the far-infrared. In Zw 049.057, infrared and optical images reveal multiple clouds in a polar dust structure, which might suggest that the outflow in this galaxy is not steady in time (Gallagher et al., in prep.). It is thus possible that, in some galaxies, we are witnessing an episodic process where the nuclear region is alternating between feedback and accretion dominated states.

Looking at the spectra presented by Veilleux et al. (2013), UGC 5101 and IRAS 17208–0014 even exhibit weak blueshifted line wings in the OH 119 μm absorption lines. This indicates the presence of gas moving toward us, but as the absorptions at negative velocities are shallow, they do not have a strong effect on the median velocities of the lines. As discussed by González-Alfonso et al. (2017a), this may suggest that we are witnessing collimated outflows in these sources, as opposed to the wide-angle outflows to which the OH 119 μm lines seem to be primarily sensitive. With all this in mind, it seems that the regions responsible for the bright HCN-vib emission are not destroyed by (fast) outflows in general, but rather by the kind of wide-angle outflows from the nuclear infrared-emitting region that are able to shift the median velocity of the OH 119 μm ground state lines by several hundreds of $\mathrm{km\,s^{-1}}$.

Turning to the two sources that show pure emission in the OH 119 μm doublet, I Zw 1 and NGC 7469, we note that they lack HCN-vib detections and that the upper limits to their $L_{\mathrm{HCN-vib}}/L_{\mathrm{IR}}$ ratios are among the lowest in our sample. Furthermore, NGC 7469 has also been observed in the OH 65 μm doublet, another tracer of obscured nuclei, but no absorption was detected (González-Alfonso et al. 2015). This is consistent with the results of Veilleux et al. (2013) that the sources with pure OH emission are those for which an AGN dominates the luminosity and that these objects represent a phase in which the feedback has subsided after clearing a path through the dusty surroundings.

4.1.3. Orientation effects

An alternative explanation to the distribution of galaxies in Fig. 1 is that it is produced by a simple orientation effect. For example, using the OH 119 μm doublet, Veilleux et al. (2013) found unambiguous evidence of outflows in 70% of their sources; this detection rate is consistent with all sources having molecular outflows and an average opening angle of ∼145°. The sources with no outflow signatures would then be those that are oriented approximately edge-on and have outflows perpendicular to our line of sight. It is harder to explain why these would also be the sources with bright HCN-vib emission, as the obscuration in a dusty edge-on disk would rather have the effect of lowering the visible HCN-vib flux, unless the line is masing as seen toward some circumstellar envelopes (e.g., Lucas & Cernicharo 1989; Bieging 2001; Menten et al. 2018).

However, the comparison so far is based on the HCN-vib luminosity divided by the total infrared luminosity which, because of the higher dust opacity in the infrared, is more affected by orientation effects. The infrared luminosity that we see thus depends on the orientation, with higher values for face-on galaxies. This effect may indeed be significant; for example, Efstathiou et al. (2014) estimated that the true infrared luminosity of IRAS 08572+3915 may be as high as $1.1\times10^{13}\,L_{\odot}$, more than five times higher than the value inferred assuming the luminosity is isotropic. Another possible example is Arp 220 for which the total infrared luminosity estimated from the IRAS fluxes is $\sim1.7\times10^{12}\,L_{\odot}$, while Sakamoto et al. (2017) estimated the bolometric luminosity from the western nucleus alone to be $\sim3\times10^{12}\,L_{\odot}$.

If we do not divide $L_{\mathrm{HCN-vib}}$ by the total infrared luminosity, we see that Mrk 231 has an HCN-vib luminosity comparable to those of the HCN-vib bright galaxies. However, it is still less luminous than in the ULIRGs Arp 220 W and IRAS 17208–0014 and only a factor of two or three brighter than in the LIRGs Zw 049.057, IC 860, and NGC 4418. Furthermore, none of the other sources with $v_{50} \lesssim -200\,\mathrm{km\,s^{-1}}$ have strong HCN-vib emission. Clearly, a larger sample will be required to investigate this issue further. If the distribution of sources in Fig. 1 is indeed due to an orientation effect, more sources with both strong HCN-vib emission and outflow signatures in the far-infrared OH lines should show up in an extended sample.

4.1.4. Evolution

Following Aalto et al. (2015a), we present a possible evolutionary scenario in which bright HCN-vib emission is tracing extremely obscured nuclei in a phase that occurs before the nuclear feedback is able to drive wide-angle outflows, or at least before such outflows can be observed in the far-infrared OH lines. In this scenario, the deeply embedded regions that provide the necessary conditions for HCN-vib excitation can coexist with fast collimated outflows, but are disrupted once nuclear wide-angle outflows have developed. A schematic view

of one possible version of the scenario is presented in Fig. 2. In this figure, the most obscured sources consist of a mid-infrared core, responsible for the HCN-vib emission, surrounded by an obscuring layer of cooler dust that accounts for the far-infrared emission. A central energy source is heating the dusty core through radiative trapping. Mid-infrared photons, which cannot escape the dusty environment, vibrationally excite the HCN molecules which may then undergo rotational transitions and emit (sub)millimeter photons that are able to penetrate the obscuring dust. Outflows in these objects are collimated and often so compact that they are still embedded in the outer layer of dust, and thus obscured from view in the far-infrared. In the next phase, the outflows have broken through the cooler dust layer and widened considerably, making them clearly detectable in most galaxies. As gas and dust are transported from the regions around the nucleus, the conditions in the mid-infrared core change, becoming less favorable for the excitation of HCN-vib. Finally, when a path has been cleared through the surrounding dust, OH is no longer detectable in absorption and the conditions for HCN-vib excitation in the core are no longer met.

A similar evolutionary sequence has been suggested by González-Alfonso et al. (2017b), and we note that, apart from UGC 5101, the HCN-vib luminous sources from our sample coincide with the sources in their extremely buried pre-feedback phase. It should be noted that, even if an evolutionary scenario like this applies in some cases, all sources in our sample may not be on the same evolutionary track. For example, a lot of nuclear power is required to push large columns of gas to high velocities, and LIRGs such as NGC 4418 and Zw 049.057 may therefore never develop powerful wide-angle outflows detectable in the far-infrared OH lines. Instead, they might evolve along the horizontal axis in Fig. 1.

Finally, an interesting comparison can be made with the highly collimated molecular outflows that are found around low-mass protostars in the earliest (class 0) stages of their formation (e.g., Konigl & Pudritz 2000; Codella et al. 2014). With time, gas at larger and larger angles from the outflow axis may be entrained, eventually sweeping away most of the envelope around the star (e.g., Arce & Sargent 2006). Furthermore, vibrationally excited HCN has been detected toward molecular hot cores around massive protostars using the direct *l*-type transitions, that is transitions between the *l*-type levels inside a rotational state, at centimeter wavelengths (e.g., Rolffs et al. 2011).

4.2. HCN-vib compared to other tracers of obscured nuclear regions.

As discussed in Aalto et al. (2015a), a prerequisite for the excitation of HCN-vib is the presence of warm and dusty regions, making it a good tracer of deeply buried nuclei. Following this logic, our results indicate that the most obscured nuclei lack evolved, wide-angle outflows. Interestingly, the results of González-Alfonso et al. (2017a), who used the equivalent width of the OH 65 μm doublet as a measure of the obscuration, suggest that the fastest outflows arise in some of the most obscured nuclei. These authors however point out that sources with high equivalent width in OH 65 μm do not necessarily have fast outflows. By comparing our Fig. 1 with their Fig. 4, we see that five of the six most HCN-vib luminous sources that are included in both samples also belong to the group of sources with high equivalent width but low outflow velocity, indicating that they are also obscured when using the OH 65 μm equivalent width as a measure. On the other hand, five of the sources with low HCN-vib luminosity are also found among the sources with high OH 65 μm equivalent width, indicating that they also contain obscured nuclei. It appears that the two measures trace different parts or physics of the galaxy nuclei. Indeed, González-Alfonso et al. (2017a) have stated that high equivalent widths require dust temperatures in excess of 60 K, while dust temperatures above 100 K are required for bright HCN-vib emission (Aalto et al. 2015a). It is thus possible that bright HCN-vib emission exclusively traces more obscured parts of the nuclei, where the dust is hotter.

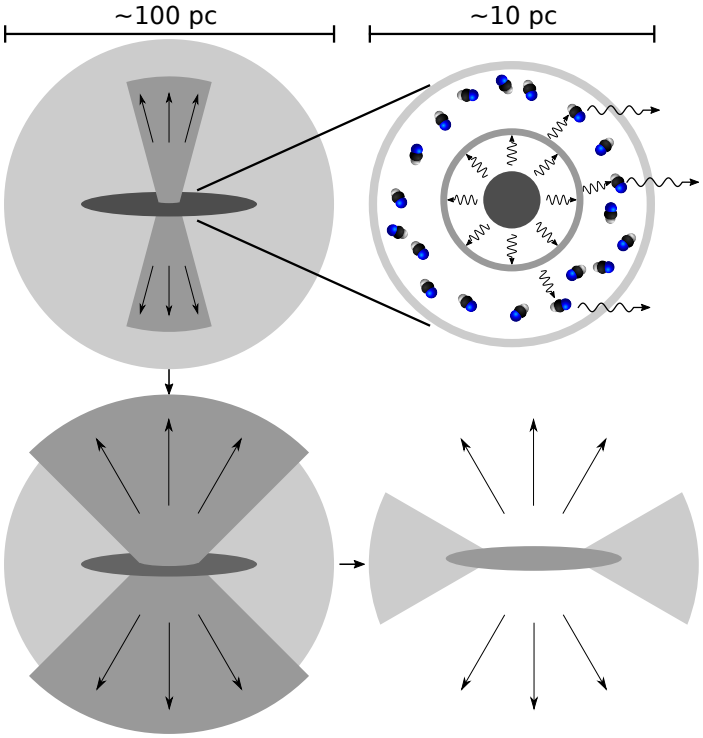

Fig. 2. Schematic view of a possible evolutionary scenario. *Upper left panel*: most obscured phase where both the mid-infrared core and the outflow are still completely embedded in a layer of cooler dust. *Upper right panel*: conditions in the mid-infrared core in this phase. *Lower left panel*: outflow has broken through the cooler layer of dust and widened, making it visible in the far-infrared. *Lower right panel*: a third stage in which the outflow has cleared a path through the surrounding dust layer. In the two final stages, conditions in the core are no longer sufficient for luminous HCN-vib emission to occur.

In a similar manner, Spoon et al. (2013) also found that the fastest outflows are found in those sources that are still deeply embedded as indicated by strong mid-infrared silicate absorptions. However, as already noted by Aalto et al. (2015a), González-Alfonso et al. (2015) found that silicate absorptions are biased toward relatively unobscured mid-infrared emitting regions, again indicating that the HCN-vib is actually tracing a more extreme form of obscuration.

5. Conclusions

We explore a possible correlation between the strength of molecular outflows in the far-infrared OH 119 μm lines and the luminosity of rotational lines of vibrationally excited HCN. A simple comparison of HCN-vib line luminosities, normalized to the total infrared luminosity of the host galaxy, and the median velocities of OH 119 μm absorption lines shows that galaxies with unusually bright HCN-vib emission tend to lack fast molecular outflows, but that galaxies without fast outflows do not necessarily have bright HCN-vib emission. This may be an

orientation effect or something that reflects a true difference between the sources, for example that the most obscured sources cannot drive wide-angle outflows or that their outflows are young and have not yet dispersed the nuclear gas and dust concentrations. Following Aalto et al. (2015a), we present an evolutionary sequence, that may apply to some of the sources, in which bright HCN-vib emission is tracing extremely obscured nuclei in a phase that occurs before the onset of wide-angle outflows. Once these massive outflows have been launched, they quickly disrupt the deeply embedded regions responsible for the bright HCN-vib emission. We note, however, that more studies are needed to extend the sample and explore the relation further. As the *Herschel* Space Observatory, which was used for the OH outflow measurements, is no longer operational, such studies should concentrate on observations of HCN-vib in galaxies that have already been observed in the OH 119 μm doublet. Another possibility is to search for hidden outflows using the radio lines of OH, either in its ground state (Baan et al. 1989) or in rotationally excited states (Falstad et al. 2018).

Acknowledgements. This paper makes use of the following ALMA data: ADS/JAO.ALMA#2015.1.00708.S, ADS/JAO.ALMA#2016.1.00140.S. ALMA is a partnership of ESO (representing its member states), NSF (USA), and NINS (Japan), together with NRC (Canada), MOST, and ASIAA (Taiwan), and KASI (Republic of Korea), in cooperation with the Republic of Chile. The Joint ALMA Observatory is operated by ESO, AUI/NRAO, and NAOJ. This research has made use of the NASA/IPAC Extragalactic Database (NED), which is operated by the Jet Propulsion Laboratory, California Institute of Technology, under contract with the National Aeronautics and Space Administration.

References

Aalto, S., Martín, S., Costagliola, F., et al. 2015a, A&A, 584, A42
Aalto, S., Garcia-Burillo, S., Muller, S., et al. 2015b, A&A, 574, A85
Aladro, R., König, S., Aalto, S., et al. 2018, A&A, 617, A20
Arce, H. G., & Sargent, A. I. 2006, ApJ, 646, 1070
Baan, W. A., Haschick, A. D., & Henkel, C. 1989, ApJ, 346, 680
Baan, W. A., Salzer, J. J., & LeWinter, R. D. 1998, ApJ, 509, 633
Barcos-Muñoz, L., Leroy, A. K., Evans, A. S., et al. 2015, ApJ, 799, 10
Barcos-Muñoz, L., Aalto, S., Thompson, T. A., et al. 2018, ApJ, 853, L28
Bieging, J. H. 2001, ApJ, 549, L125
Codella, C., Cabrit, S., Gueth, F., et al. 2014, A&A, 568, L5
Efstathiou, A., Pearson, C., Farrah, D., et al. 2014, MNRAS, 437, L16
Falstad, N., González-Alfonso, E., Aalto, S., et al. 2015, A&A, 580, A52
Falstad, N., González-Alfonso, E., Aalto, S., & Fischer, J. 2017, A&A, 597, A105
Falstad, N., Aalto, S., Mangum, J. G., et al. 2018, A&A, 609, A75
Ferrarese, L., & Merritt, D. 2000, ApJ, 539, L9
Fischer, J., Sturm, E., González-Alfonso, E., et al. 2010, A&A, 518, L41
Fluetsch, A., Maiolino, R., Carniani, S., et al. 2018, MNRAS, submitted [arXiv:1805.05352]
García-Burillo, S., Combes, F., Usero, A., et al. 2015, A&A, 580, A35
Gebhardt, K., Bender, R., Bower, G., et al. 2000, ApJ, 539, L13
Ginsburg, A., & Mirocha, J. 2011, Astrophysics Source Code Library [record ascl:1109.001]
Goicoechea, J. R., Joblin, C., Contursi, A., et al. 2011, A&A, 530, L16
González-Alfonso, E., Fischer, J., Graciá-Carpio, J., et al. 2012, A&A, 541, A4
González-Alfonso, E., Fischer, J., Sturm, E., et al. 2015, ApJ, 800, 69
González-Alfonso, E., Fischer, J., Spoon, H. W. W., et al. 2017a, ApJ, 836, 11
González-Alfonso, E., Armus, L., Carrera, F. J., et al. 2017b, PASA, 34, e054
Hopkins, P. F., Hernquist, L., Cox, T. J., Robertson, B., & Springel, V. 2006, ApJS, 163, 50
Hughes, D. H., Serjeant, S., Dunlop, J., et al. 1998, Nature, 394, 241
Imanishi, M., & Nakanishi, K. 2013, AJ, 146, 91
Imanishi, M., Nakanishi, K., & Izumi, T. 2016a, AJ, 152, 218
Imanishi, M., Nakanishi, K., & Izumi, T. 2016b, ApJ, 825, 44
Imanishi, M., Nakanishi, K., & Izumi, T. 2018, ApJ, 856, 143
Kim, D.-C., Veilleux, S., & Sanders, D. B. 1998, ApJ, 508, 627
Konigl, A., & Pudritz, R. E. 2000, Protostars and Planets IV, 759
Kormendy, J., & Ho, L. C. 2013, ARA&A, 51, 511
Lahuis, F., Spoon, H. W. W., Tielens, A. G. G. M., et al. 2007, ApJ, 659, 296
Lucas, R., & Cernicharo, J. 1989, A&A, 218, L20
Magorrian, J., Tremaine, S., Richstone, D., et al. 1998, AJ, 115, 2285
Maloney, P. R., Hollenbach, D. J., & Tielens, A. G. G. M. 1996, ApJ, 466, 561
Martín, S., Aalto, S., Sakamoto, K., et al. 2016, A&A, 590, A25
McMullin, J. P., Waters, B., Schiebel, D., Young, W., & Golap, K. 2007, ASP Conf. Ser., 376, 127
Meijerink, R., Spaans, M., Loenen, A. F., & van der Werf, P. P. 2011, A&A, 525, A119
Menten, K. M., Wyrowski, F., Keller, D., & Kamiński, T. 2018, A&A, 613, A49
Moshir, M., Kopman, G., & Conrow, T. A. O. 1992, IRAS Faint Source Survey, Explanatory Supplement Version 2
Ott, S. 2010, ASP Conf. Ser., 434, 139
Pérault, M. 1987, PhD Thesis, PhD dissertation, Université Paris VII, France
Pilbratt, G. L., Riedinger, J. R., Passvogel, T., et al. 2010, A&A, 518, L1
Poglitsch, A., Waelkens, C., Geis, N., et al. 2010, A&A, 518, L2
Privon, G. C., Aalto, S., Falstad, N., et al. 2017, ApJ, 835, 213
Rolffs, R., Schilke, P., Wyrowski, F., et al. 2011, A&A, 529, A76
Sakamoto, K., Aalto, S., Wilner, D. J., et al. 2009, ApJ, 700, L104
Sakamoto, K., Aalto, S., Evans, A. S., Wiedner, M. C., & Wilner, D. J. 2010, ApJ, 725, L228
Sakamoto, K., Aalto, S., Barcos-Muñoz, L., et al. 2017, ApJ, 849, 14
Sanders, D. B., & Mirabel, I. F. 1996, ARA&A, 34, 749
Sanders, D. B., Soifer, B. T., Elias, J. H., et al. 1988a, ApJ, 325, 74
Sanders, D. B., Soifer, B. T., Elias, J. H., Neugebauer, G., & Matthews, K. 1988b, ApJ, 328, L35
Sanders, D. B., Phinney, E. S., Neugebauer, G., Soifer, B. T., & Matthews, K. 1989, ApJ, 347, 29
Sanders, D. B., Scoville, N. Z., & Soifer, B. T. 1991, ApJ, 370, 158
Sanders, D. B., Mazzarella, J. M., Kim, D.-C., Surace, J. A., & Soifer, B. T. 2003, AJ, 126, 1607
Simpson, J. M., Smail, I., Swinbank, A. M., et al. 2012, MNRAS, 426, 3201
Smail, I., Ivison, R. J., & Blain, A. W. 1997, ApJ, 490, L5
Solomon, P. M., & Vanden Bout, P. A. 2005, ARA&A, 43, 677
Spilker, J. S., Aravena, M., Béthermin, M., et al. 2018, Science, 361, 1016
Spoon, H. W. W., Farrah, D., Lebouteiller, V., et al. 2013, ApJ, 775, 127
Strauss, M. A., Huchra, J. P., Davis, M., et al. 1992, ApJS, 83, 29
Urrutia, T., Lacy, M., & Becker, R. H. 2008, ApJ, 674, 80
Veilleux, S., Kim, D.-C., Sanders, D. B., Mazzarella, J. M., & Soifer, B. T. 1995, ApJS, 98, 171
Veilleux, S., Meléndez, M., Sturm, E., et al. 2013, ApJ, 776, 27
Véron-Cetty, M.-P., & Véron, P. 2001, A&A, 374, 92

Appendix A: Vibrationally excited HCN in IRAS 15250+3609

The ULIRG IRAS 15250+3609 was observed in the HCO^+ J = 3−2 line by Imanishi et al. (2016a). They interpreted a peak close to the expected position of the HCN-vib line as an outflow signature in the HCO^+ line. Their interpretation is supported by the fact that similar features are seen in the HCN J = 3−2 and J = 4−3 lines (Imanishi et al. 2016a, 2018). However, relative to the main lines, the subpeak close to the HCO^+ line is stronger than that close to the HCN line. This could be because of differing abundances or excitation in the outflowing gas but it could also be a contribution from HCN-vib. Furthermore, IRAS-15250+3609 has a high equivalent width in the OH 65-μm doublet (González-Alfonso et al. 2015), indicating that the galaxy is highly obscured, as well as an HCN absorption at 14-μm (Lahuis et al. 2007). In this work, we attributed the feature as completely due to HCN-vib emission, but it is likely that it is indeed blended with an HCO^+ outflow signature and the value given should be considered an upper limit to the HCN-vib luminosity.

Appendix B: Previously unpublished HCN-vib detections

We found two sources with previously unpublished detections of HCN-vib in the ALMA science archive, i.e., IRAS 12224–0624 (project 2015.1.00708.S, PI: L. Armus) and IRAS 05189–2524 (project 2016.1.00140.S, PI: D. Iono). The observations of IRAS 05189–2524 were conducted during two runs on 2016 November 12 and 15 with a total of 42 antennas with baseline lengths ranging between 15.1 m and 1.0 km. A spectral window centered at 341.8 GHz covered a bandwidth of 1.875 GHz (~1650 km s^{-1} at the frequency of HCN-vib J = 4−3) and the frequency resolution was 3.9 MHz. During both runs J0522–3627 was used as bandpass and flux calibrator, and J0457–2324 was used as phase calibrator. The total on-source time of the observations was 3340 s and the final sensitivity achieved was 0.5 mJy beam^{-1} per 20 km s^{-1} (~24 MHz) channel. For the imaging we used Briggs weighting with a robustness factor of 0.5. The resulting beam size is 0.29″ × 0.22″ (PA ~ 63°).

The observations of IRAS 12224–0624 were conducted during a single run on 2016 April 27 with a total of 38 antennas with baseline lengths ranging between 15.1 m and 452.8 m. A spectral window centered at 347.4 GHz covered a bandwidth of 1.875 GHz (~1600 km s^{-1} at the frequency of HCN-vib J = 4−3) and the frequency resolution was 3.9 MHz. The calibrators used were J1256–0547, which was used for bandpass and flux calibration, and J1246–0730, which was used for phase calibration. The total on-source time of the observations was 395 s and the final sensitivity achieved was 1.5 mJy beam^{-1} per 20 km s^{-1} (~24 MHz) channel. For the imaging we used Briggs weighting with a robustness factor of 0.5. The resulting beam size is 0.51″ × 0.44″ (PA ~ 82°).

For both sources, the Common Astronomy Software Applications (CASA; McMullin et al. 2007) package was used to reapply the calibration and perform imaging. The line fluxes used to calculate the HCN-vib luminosities were then found by fitting Gaussians to the HCO^+ and HCN-vib lines in spectra that were spatially integrated over the sources. These spectra are presented in Fig. B.1. We note that the wavelengths of the HCO^+ and HCN-vib lines in IRAS 05189–2524 are offset from those expected when using the redshift of 0.0426 adopted by Veilleux et al. (2013). They are however consistent with the redshift of ~0.0428 found from the CO J = 1−0 observations reported by Sanders et al. (1991). Using this redshift instead of that adopted by Veilleux et al. (2013) to determine the median OH absorption velocity results in an extra velocity shift of −45 km s^{-1}.

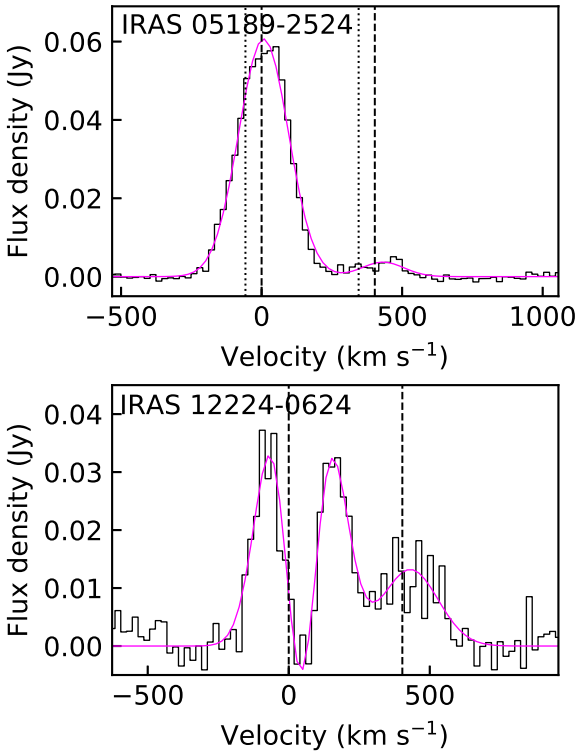

Fig. B.1. Spectral fits to the HCO^+ and HCN-vib J = 4−3 lines in the two galaxies IRAS 05189–2524 and IRAS 12224–0624. The solid black histograms represent the data and the solid magenta lines indicate the best fits to the data. The velocity scale is set relative to the frequency of the HCO^+ J = 4−3 line. Dashed vertical lines indicate the expected positions of the HCO^+ and HCN-vib J = 4−3 lines given the adopted redshifts. The dotted lines in the plot for IRAS 05189–2524 indicate the expected positions given the redshift adopted by Veilleux et al. (2013).

Appendix C: New OH outflow measurements

Three of the sources with existing HCN-vib observations also had observations of the OH doublet at 119 μm taken with the Photodetector Array Camera and Spectrometer (PACS; Poglitsch et al. 2010) on *Herschel* but were not included in the sample of Veilleux et al. (2013). The observations of Zw 049.057 (OBSID: 1342248368, PI: E. González-Alfonso) were conducted on 2012 July 20 for a duration of 1478 s, the observations of IRAS 20414–1651 (OBSID: 1342217908, PI: D. Farrah) were conducted on 2011 April 5 for a duration of 8879 s, and the observations of NGC 7469 (OBSID: 1342235840, PI: E. González-Alfonso) were conducted on 2011 December 31 for a duration of 1086 s. All observations were performed in high spectral sampling, range spectroscopy mode. The observations had been processed with version 14.2 of the standard pipeline and were not in need of reprocessing. In all sources, the nuclear far-IR emission is spatially unresolved in the central 9.4″ (~2 kpc) spaxel of the PACS 5 × 5 spaxel array. As the central PACS spaxel is smaller than the point spread function of the spectrometer, the spectrum was extracted using the point source correction task in the *Herschel* interactive processing environment (HIPE; Ott 2010) version 14.0.1. Before

analyzing the absorption lines, polynomials of order two were fitted to the continuum and then subtracted from the spectra. For consistency, the profiles of the 119 μm OH doublets were modeled using the same procedure as in Veilleux et al. (2013). Each line was fitted with two Gaussian components characterized by their amplitude, position, and width. The separation between the two lines of the doublet was fixed at 0.208 μm in the rest frame and the amplitude and width of the two lines were the same for each component. The median velocities of the absorptions (v_{50}(abs)) were then determined from these fits. The fitting procedure was carried out using the spectroscopic analysis toolkit *PySpecKit* (Ginsburg & Mirocha 2011) and the continuum subtracted spectra with the fits overplotted are presented in Fig. C.1.

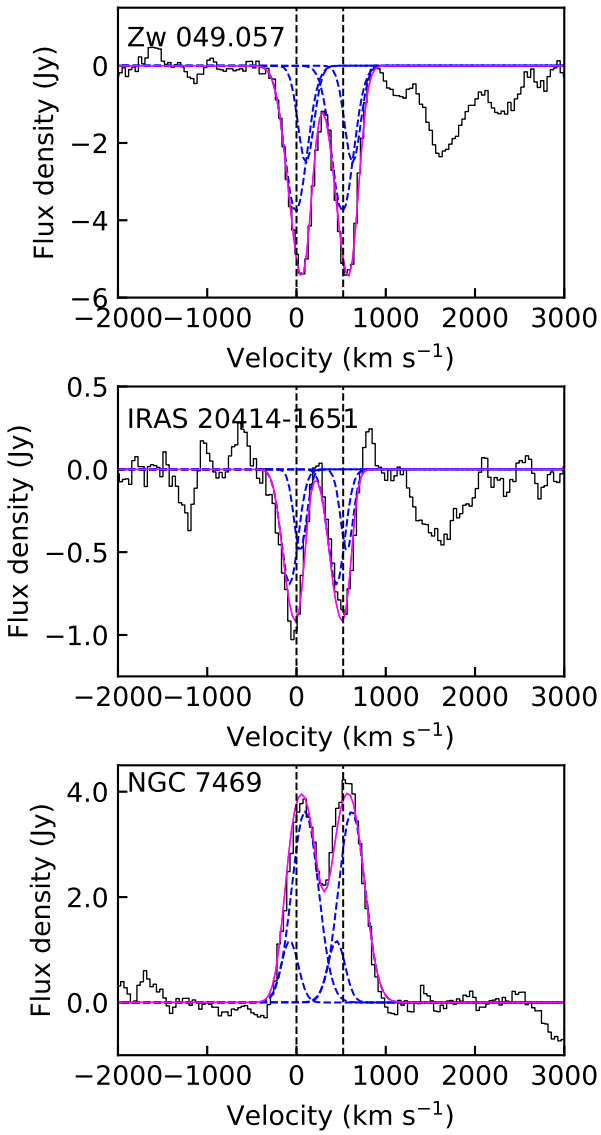

Fig. C.1. Spectral fits to the OH 119 μm absorption lines in the galaxies Zw 049.057, IRAS 20414–1651, and NGC 7469. The solid black histograms represent the data, the solid magenta lines indicate the best multicomponent fits to the data, and the dashed blue lines represent the individual components. The velocity scale is set relative to the frequency of the blue component of the doublet. Dashed vertical lines indicate the expected positions of the two absorption components given the adopted redshifts.